Time-dependent optimization of laser-produced molecular plasmas through high-order harmonic generation

Ganjaboy S. Boltaev (iD), Rashid A. Ganeev (iD), Vyacheslav V. Kim (iD), Ke Zhang (iD), Mottamchetty Venkatesh, and Chunlei Guo

View Online   Export Citation   CrossMark

Time-dependent optimization of laser-produced molecular plasmas through high-order harmonic generation

View Online   Export Citation   CrossMark

Ganjaboy S. Boltaev,[1,2] (iD) Rashid A. Ganeev,[1,2,3,a] (iD) Vyacheslav V. Kim,[1,2] (iD) Ke Zhang,[1] (iD) Mottamchetty Venkatesh,[1] and Chunlei Guo[1,4,a]

AFFILIATIONS

[1] The Guo China-US Photonics Laboratory, State Key Laboratory of Applied Optics, Changchun Institute of Optics, Fine Mechanics and Physics, Chinese Academy of Sciences, Changchun 130033, China
[2] Department of Physics, American University of Sharjah, PO Box 26666, Sharjah, United Arab Emirates
[3] Faculty of Physics, Voronezh State University, 1 University Square, Voronezh 394006, Russia
[4] The Institute of Optics, University of Rochester, Rochester, New York 14627, USA

[a]Authors to whom correspondence should be addressed: rashid_ganeev@mail.ru and guo@optics.rochester.edu

ABSTRACT

Analysis and characterization of laser-produced plasmas (LPPs) require the advanced methods for determination of different multiparticle component formation and spreading. Time-resolved high-order harmonic generation (HHG) in spreading LPPs allows determining optimal conditions for this process. One of the most important parameters of HHG in LPP is the delay between the heating and driving pulses. We demonstrate that the optimization of delays allows achieving the maximal harmonic yields in LPP created on the surfaces of the solid targets possessing different molar masses (m). The optimal delays (t) for B_4C, ZnO, GaP, GaAs, and Ag_2S plasmas were determined to be approximately 200, 300, 350, 500, and 700 ns, respectively. These variations of delays correspond to the $t \infty (m)^{0.5}$ dependence for different materials. We demonstrate the applicability of the proposed method for analysis of the resonance-enhanced harmonics in atomic and molecular plasmas (Mo and MoS_2) and for studies of large perovskite aggregates as potential emitters of harmonics. This diagnostic technique can also be applied to the analysis of the presence of different nanostructures in LPPs through HHG with a high spatiotemporal resolution.

Published under license by AIP Publishing. https://doi.org/10.1063/1.5123244

High-order harmonic generation (HHG) of ultrashort laser pulses in an isotropic medium is a nonlinear optical method for the generation of coherent extreme ultraviolet (XUV) radiation. Various theoretical and experimental studies have been devoted to increasing HHG conversion efficiency.[1,2] HHG in gases, laser-produced plasmas (LPPs), and solid surfaces demonstrate the possibility of attosecond pulse generation in the XUV range.[3] Early studies of HHG in molecular species were considered as a spectroscopy tool.[4] The analysis of HHG spectra can be useful for indication of the alignment of molecules at different angles, which show the signatures of the molecular structure. HHG spectroscopy can also be considered as a method for analysis of the complex biomolecules. The ablation of the molecules is also important for the enhancement of HHG efficiency.[5]

The low-excited and low-ionized laser plasma plumes can be considered as the suitable media for efficient generation of high-order harmonics (HH), allowing demonstration of the resonance enhancement of single harmonic, quasi-phase matching in multijet plasmas and nanoparticle-enhanced harmonics.[6–15] Various LPPs were considered as the nonlinear optical media for generation of the low- and high-order harmonics of picosecond and femtosecond driving pulses.[16] The harmonic cutoff in the case of the targets with different atomic numbers shows the strong dependence on the delay between the heating and driving pulses. In those experiments, the optimization of plasma parameters and delay between ablating and driving pulses led to the growth of the harmonic yield.[17] The correlation between those results and the appearance of a second component of the third harmonic (TH) at longer delays confirmed the presence of aggregates in the graphite plasma and established the analysis of their presence in LPPs with an excellent spatiotemporal resolution through the harmonic generation.[18]

There are a few techniques, which were used for analysis of the composition and dynamics of LPPs. Optical emission spectroscopy

(OES) and time-of-flight mass spectrometry (TOF-MS) stand as some of the most used methods of plasma characterization.[19] Laser-induced breakdown spectroscopy (LIBS) allows indicating and distinguishing different plasma species by their emission spectra during excitation of targets by nanosecond pulses.[20] The information retrieved by OES from the spontaneous emission of LPPs allows determining important parameters of plasma formation, such as the electron temperature and density, while TOF-MS provides the information about the presence of ions in LPP.[21]

In this paper, we analyze the dynamics of plasma formation using the molecular bulk targets possessing different molar masses at the conditions of the maximal HH yield along a broad range of delays between the heating nanosecond and driving femtosecond pulses. We show that the optimization of the HH yield strongly depends on the delay between heating and driving pulses and correspondingly depends on the molar weights of different species presented in LPP. Different applications of this method of the nonlinear optical characterization of LPPs are described.

The experimental setup of HHG in LPPs using a two-laser configuration is shown in Fig. 1. This technique has recently been introduced to determine the role of clusters in HHG.[22] The key feature of the two-laser configuration is a possibility to control the delay time between heating nanosecond pulses and driving femtosecond pulses over a long range using a digital generator (DG535, Stanford Research Systems). The delay between the heating and driving pulses was monitored on an oscilloscope using a fast photodiode. The radiation of the Ti:Sapphire laser ($\lambda = 800$ nm, $\tau = 40$ fs, 1 kHz; Spitfire Ace, Spectra-Physics) was used for interaction with the laser plasma produced by the Nd:YAG laser (1064 nm, 5 ns, 10 Hz; Q-Smart 850, Coherent), leading to the generation of harmonics.

The laser plasma plumes were created on the surfaces of different targets using the nanosecond Nd:YAG laser. The diameter of the ablation zone was 0.5 mm. The fluence of 10 mJ, 5 ns heating pulses on the target surface was 4 J/cm². The position of the target with regard to the optical axis of propagation of the driving femtosecond pulses was controlled by the microtranslating stage to achieve the maximal efficiency in the conversion of the driving pulse energy to the harmonics yield. The step of the microtranslating stage was equal to 0.1 mm. The femtosecond driving pulses were focused by a 300 mm focal length lens at a distance of ~1 mm above the surface of solid targets, which was optimal to achieve a relatively high yield of HH generated in the plasma plumes. An electronic delay between the heating (nanosecond) and driving (femtosecond) pulses was varied between 0 and 5000 ns though it can also be extended up to 50 μs to determine the influence

of large aggregates in LPPs on HHG. The harmonic spectra were analyzed using an extreme ultraviolet spectrometer.

The B_4C, ZnO, GaP, ZnS, GaAs, CdS, Ag_2S, MoS_2, and $CH_3NH_3PbBr_3$ samples with different molar weights were used as the targets for ablation and plasma formation for HHG. The sizes of all targets were $5 \times 5 \times 2$ cm³. The ablation of targets was carried out in the vacuum chamber at 2.5×10^{-4} Pa. The targets were chosen by the difference in their molar weight to analyze the influence of different components on HHG efficiency.

The velocity of plasma species depends on the atomic or molecular weight of the particles. Figure 2 shows spectra of the harmonics generated in the plasma plumes produced on the B_4C and ZnO targets ablated using 5 ns, 1064 nm pulses. In the case of ZnO plasma (84 g/mol), the harmonics up to the 23rd order of 800 nm, 40 fs pulses were achieved. The plasma containing B_4C (55 g/mol) allowed observing the harmonics up to the 15th order at the same experimental conditions of ablation and driving beam propagation [Fig. 2(a)].

The variation of harmonic intensity depends on the delay between the heating nanosecond and driving femtosecond pulses, as shown in Fig. 2(b). The optimal delays allowing generation of the strongest 9th harmonic were found to be 300 and 200 ns for ZnO and B_4C plasmas. One can see the shift of the maximal yield of the 9th harmonic toward the longer delay in the case of the plasma containing heavier particles (ZnO) with regard to lighter ones (B_4C). Other harmonics from those plasmas also showed the analogous dependence.

Similar dependences of the optimal delay on the molecular weight of the components of plasmas were observed in the cases of different groups of ablating targets. Figures 2(c) and 2(d) show the comparative harmonic spectra and delay dependences of the 13th harmonic for GaP (101 g/mol) and GaAs (145 g/mol) plasma plumes. The same delay-dependent optimization of harmonics was obtained in the case of ZnS (97 g/mol) and CdS (144 g/mol) plasmas. The delay dependences of the lower-order harmonics generating in the plasmas produced during ablation of ZnS were also analyzed in Ref. 23. For the 3rd to 7th orders, the maximum harmonic yields were obtained at around 250 ns, which means the generation of harmonics from the ZnS molecules.

Figure 3(a) shows the harmonic spectrum generated in the silver sulfide LPP. This plasma allowed generation of the harmonics up to the 39th order. Here, we also analyzed the variation of the intensity of the 11th harmonic generated in this plasma by changing the delay between heating and driving pulses [Fig. 3(b)]. The maximum yields of the 11th harmonic were observed at delays of 140 and 700 ns. These delays correspond to the contributions of Ag (108 g/mol) ions and neutrals and Ag_2S (248 g/mol) ions and molecules to the harmonic
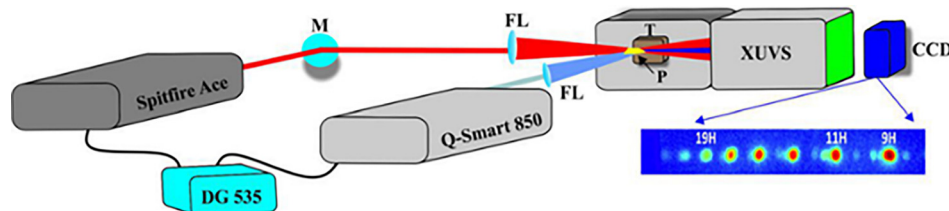

FIG. 1. Setup for high-order harmonic generation using a synchronized two-laser system. Spitfire Ace, femtosecond laser; Q-Smart 850, nanosecond laser; DG535, delay generator; M, mirror; FL; focusing lenses; T, targets; P, plasmas; XUVS, XUV spectrometer; and CCD, CCD camera. The inset shows the raw image of the HHG spectrum generated in ZnO plasma.
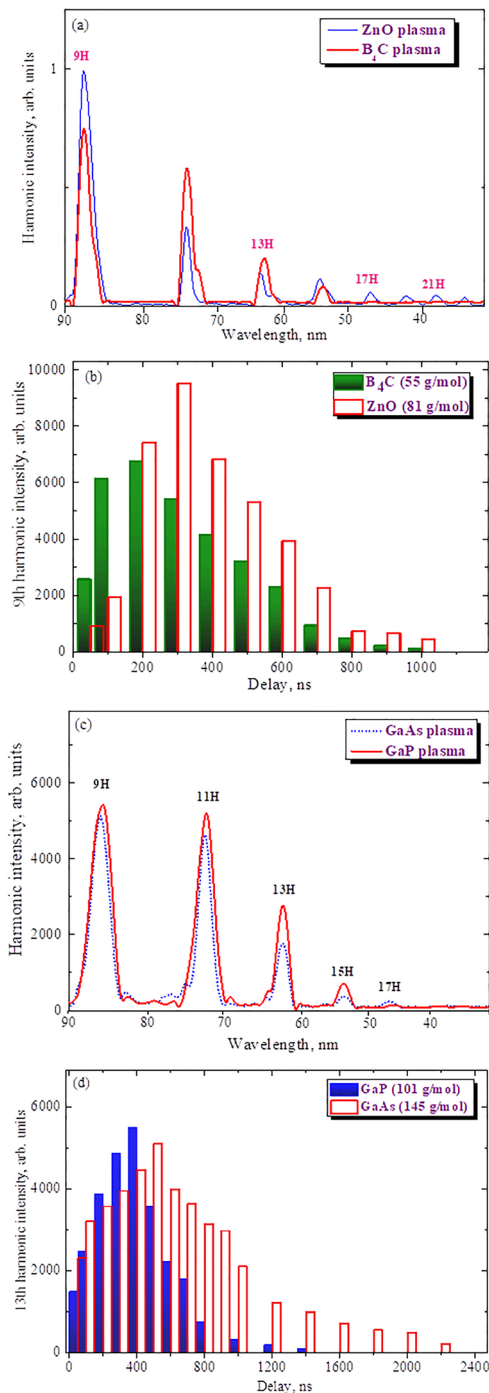
FIG. 2. (a) Spectra of the harmonics generated in B$_4$C and ZnO plasmas. (b) Variations of intensity of the 9th harmonic generated in B$_4$C and ZnO plasmas at different delays between the heating 1064 nm, 5 ns pulses and driving 800 nm, 40 pulses. The maximal yields of the 9th harmonic were obtained at delays of 200 and 300 ns for B$_4$C and ZnO plasmas, respectively. (c) Harmonic spectra obtained from GaP and GaAs plasmas. (d) Dependences of the intensity of the 13th harmonic on the delay between the heating and driving pulses in the cases of GaP and GaAs plasmas. In these cases, the longer optimal delay time corresponded to heavier molecules (GaAs).
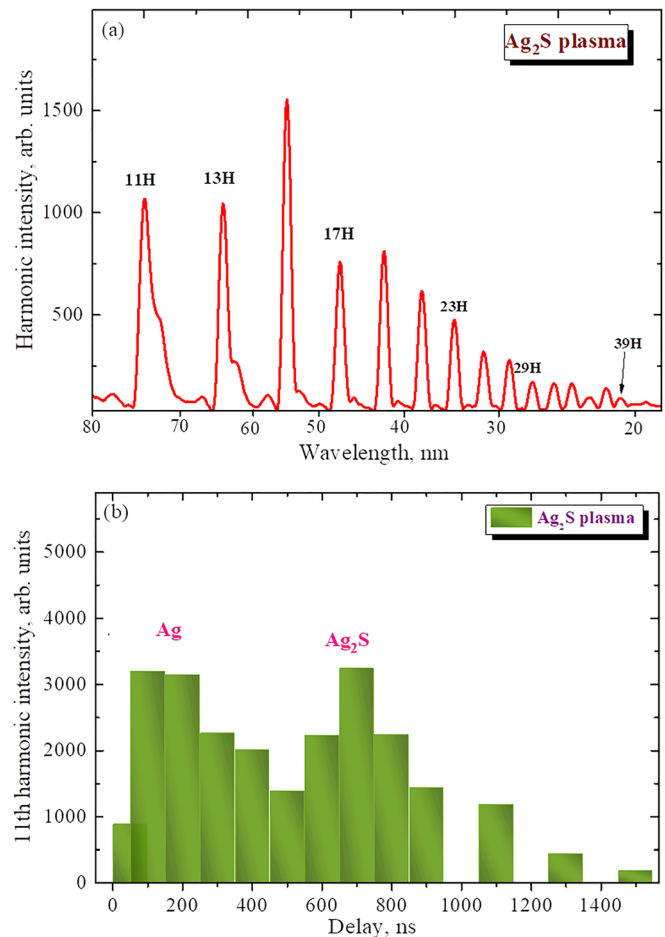

FIG. 3. (a) Harmonic spectrum generated in LPP produced on the Ag$_2$S target by 1064 nm, 5 ns pulses. (b) Variations of the 11th harmonic intensity at different delays between the heating and driving pulses in the Ag$_2$S LPP. Two peaks of the maximal intensity of the 11th harmonic were observed in the case of HHG in Ag$_2$S target ablation (at delays of ∼140 and 700 ns).

yield. During ablation of the Ag$_2$S target at relatively large fluencies of heating pulses, the molecules can be partially disintegrated to form the groups of Ag and Ag$_2$S plasma clouds, which arrived at different times at the area of interaction with the driving pulses.

The optimization of HHG strongly depends on the position of the sample with regard to the optical axis of the driving pulses. The delay dependence for different positions of targets has been discussed in Ref. 5. The intensity of the harmonics generated from atoms rapidly decreased with the growth of the distance from the optical axis to the target. For each distance, the optimum delay between the ablating laser pulse and the fundamental pulse allowing generation of strongest harmonics was found. Meanwhile, clusters and nanoaggregates can contribute to HH efficiency at notably longer delays (up to 40 μs).

In the present study, we analyzed the variation of the optimal delay at the same distance for different targets. The analysis of HHG allows determining the optimal delay during laser ablation using the nanosecond heating pulses. The studies of the ablated plasma

expansion using pulses of different durations have shown the variation of the sizes of plasma in the case of ablation by the nanosecond pulses.[24] In the case of femtosecond pulses, the dimensions of plasma plumes remain unchanged. Typical spectral- and time-integrated two-dimensional images of the nanosecond and femtosecond induced LPPs recorded using ICCD have clearly demonstrated the difference in the hydrodynamics of these two plasma plumes. Under similar ablation conditions, the spatial extension of the femtosecond LPP in the direction along the normal to the target was found to be longer compared to the nanosecond pulse induced LPP. This behavior can influence the conversion efficiency of the HH, which directly depends on the concentration of the ablated plasma species.

The velocities of the components of ablated plume can be estimated as d/t, where t is the optimal delay corresponding to the maximal harmonic yield and d is the distance between the target surface and the axis of femtosecond beam propagation. During the ablation using stronger pulses, the larger amount of the components of disintegrated molecules leaves the target surface. The produced atoms eject faster from surfaces of the target and reach the driving beam at a shorter time [Fig. 3(b)]. Variable fluence of heating pulses can change the plasma dynamics of targets.[25] This behavior has earlier been analyzed for ejected Sn particles, which possessed a velocity of 10 km/s in the case of plasma formation using the nanosecond pulses.[25] In our case, we also used the 1064 nm, 5 ns heating pulses and the plasma plumes mainly consisted of the molecules, neutral atoms, and single charged particles.

Based on the kinetic theory, the velocity of particles can be described as[26]

$$v = (2E/m)^{0.5}. \tag{1}$$

Here, E is the kinetic energy of particles and m is the mass of particles (atoms or molecules). Correspondingly, the arrival time of the plasma at the distance d above the target surface is described by

$$t \propto d/v \propto (m)^{0.5}. \tag{2}$$

Figure 4 shows the dependence of the optimal delay between the heating and driving pulses on the molecular weight of the studied molecular species. Here, we also present the theoretical $t \propto (m)^{0.5}$ dependence, which shows the reasonable coincidence with the experimental data taking into account the accuracy in the determination of the optimal delay (30%). The fitting data were plotted for distances ≤ 1 mm between the target surface and the optical axis of the driving femtosecond laser pulses.

Some deviation from the theoretical dependence could be attributed to larger laser fluence required for evaporation of the species possessing a smaller molar weight.[26–28] The plasma components possessing higher velocity reach the interaction zone with driving pulses during the shorter period. In some cases, the formation of clusters can also influence the velocity of plasma species during laser ablation using nanosecond pulses.

The developed technique is based on the two-laser approach, when two lasers emit the pulses synchronized with each other. In that case, the application of the digital delay generator allowed us to tune the delay between heating and driving pulses by the electronic method rather by the optical one. Moreover, this method allows significant broadening of the range of delay variations (up to tens
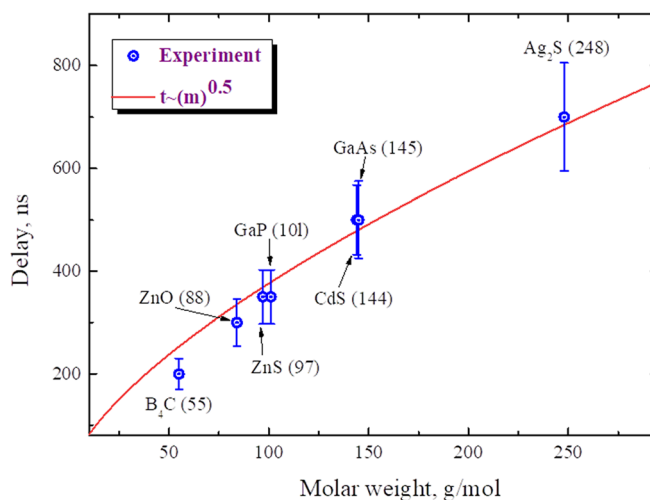

FIG. 4. Variation of the optimal delay between the heating and driving pulses on the molar weight of ablated molecules (empty circles). The theoretical fit is plotted based on the kinetic theory of particle distribution by velocity (solid line).

of microseconds). This notably larger range of delay variations becomes extremely useful once one considers the analysis of the movement of not only molecular species but also the larger-sized species (clusters, quantum dots, and even large nanoparticles) being ablated on the surfaces of targets. The optical method of delay variations used in previous studies of HHG in laser-produced plasmas is useless in that case. The additional advantage of the proposed method is the maintenance of the same characteristics of the driving beam entering the plasma volume.

The advancement presented in this study is the development of the above approach, which is not restricted only with the technical amendment yet demonstrated by other researchers but rather uses it for the analysis of the dynamics of different morphological components during laser ablation and their role in the conversion of IR femtosecond pulses toward the XUV. The timeliness of this approach is related to the recent studies of the role of different multiparticle species during the enhanced harmonics generation in plasma.[22] Notice the absence of studies on the microsecond time scale of delays assuming the hypothesis of the slower velocities for larger-sized species. The only way to investigate this optimization is the application of the electronically driven delay variations. The importance of the suggested approach can be further emphasized in the case of the multiparticle systems.

Apart from this novelty, we demonstrated the analysis of ablated molecular species for HHG. The example is presented in Fig. 3(b), which shows that, at relatively strong ablation, the disintegration of molecular species leads to optimization of HHG at different delays attributed to the specific components of those molecules.

The well-developed three-step model of HHG in gases and plasmas[29–31] can describe some peculiarities of our studies. The recombination time of the excited electron depends on the wavelength of the driving femtosecond pulses. The resonance enhancement of single high-order harmonic relies on the transitions of ions or atoms and molecules possessing strong oscillator strength close to the wavelength of some harmonics. This approach has been earlier summarized as a

four-step model for the analysis of the observed peculiarities of single harmonic enhancement in different plasmas.[12,32,33] Meanwhile, in the present case, the optimization of HHG was achieved through the analysis of the dynamics of plasma spreading rather than using the fundamental processes of HHG and resonance enhancement.

The present approach that allows the manipulation of the delay between pulses by electronic rather than optical methods opens up new opportunities in the analysis of the spreading of different components of plasma. It also gives the clues on how and when large aggregates, like clusters and quantum dots, can be involved in HHG. The two-laser approach may open the possibility to electronically control the delay time between ablating and driving pulses in the case of the large nanoparticles spreading out from the ablated surfaces. Notice that the details of the theoretical studies of velocity variations of the species ablated from the materials possessing different molar weights were reported in Refs. 24–28. Thus, the developed experimental approach allows the broadening of the area of plasma component studies through the nonlinear optical methods at longer timescales from the beginning of plasma formation during laser ablation.

The importance of the new technique is justified with its application for the studies of, for instance, the resonance processes in molecular plasmas, as well as the analysis of perovskite quantum dots and large molecules. Since the developed approach allows the consideration of slowly moving heavy plasma species, alongside the fast moving atoms, the comparative studies of light and heavy plasma components offer the analysis of different physical processes in plasmas. Among them, one can consider the resonance enhancement of single harmonic from variable plasma constituents, comparison of the efficiency of quantum dot harmonic emitters possessing different masses, etc.

First, such an example is related to the resonance processes during HHG, leading to the enhancement of the single harmonic over the neighboring ones. The mechanism of resonance-induced enhancement of single harmonic described by the four-step model[32] allowed determining the conditions at which this process occurs in the metal plasmas such as In, Cr, and Mn.[16] Earlier, only GaAs molecular plasma has demonstrated a similar process when the 21st harmonic of the 800 nm pump showed a stronger yield than the neighboring harmonics.[34] Our present experiments with MoS_2 plasma did not show the resonance enhancement of single harmonic during the formation of plasma at relatively small fluence of heating pulses [2 J cm^{-2}; Fig. 5(a), thick curve]. Meanwhile, similar experiments using the atomic target (Mo) allowed the observation of the resonantly enhanced 25th harmonic, which was notably stronger than the 21st, 23rd, 27th, and 29th harmonics [Fig. 5(a), thin curve].

This process was attributed to the closeness of the wavelength of the 25th harmonic and the wavelength of Mo ionic transition possessing large oscillator strength. The absence of a similar effect in MoS_2 plasma was probably caused by the shift of the wavelength of the above transition in this molecule out from the wavelength of the 25th harmonic ($\lambda = 32$ nm). The application of the two-laser scheme allowed achieving maximal harmonic yields from Mo and MoS_2 plasmas at the delays of femtosecond pulses ∼300 and 400 ns from the beginning of the ablation of those materials [Fig. 5(b)]. The square root of the ratio of molar and atomic masses of MoS_2 and Mo (∼1.3) approximately corresponds to the ratio of the optimal delays for these plasmas, thus confirming the above consideration of this process using different species. The ablation of the molecular target at larger fluence of heating
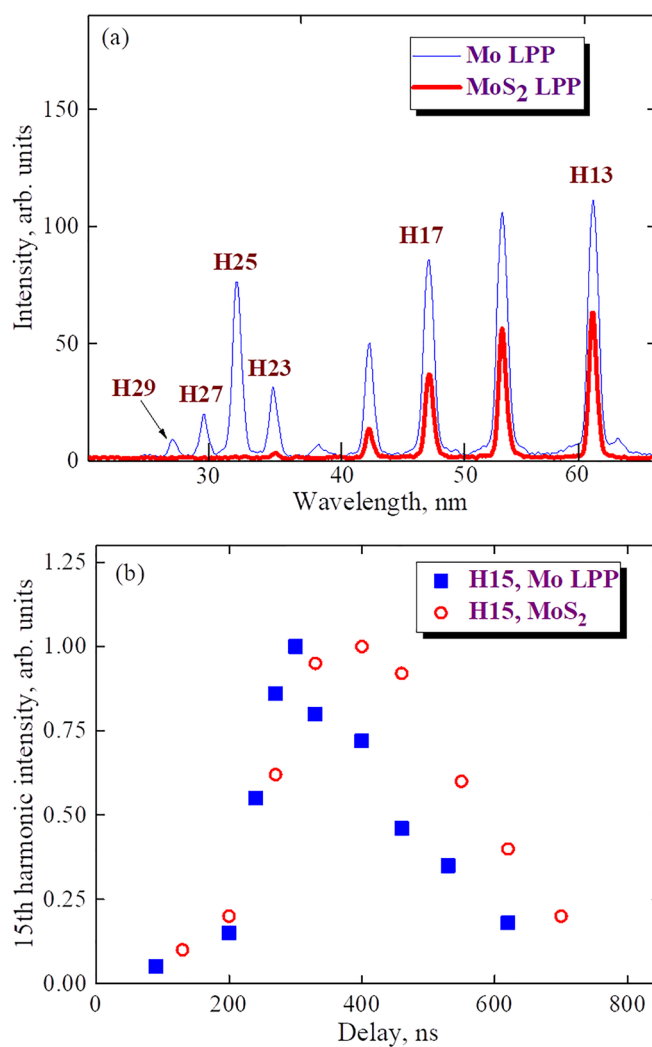

FIG. 5. (a) Harmonic spectra of Mo (thin curve) and MoS_2 (thick curve) LPPs. (b) Normalized 15th harmonic yields from Mo (filled squares) and MoS_2 (empty circles) at different delays between heating and driving pulses.

pulses (4 J cm^{-2}) led to broadening of the delay-dependent curve for MoS_2, thus indicating the partial disintegration of this molecule on Mo and S components. The latter component does not notably influence the harmonic yield, while the appearance of Mo ions allowed observation of the enhanced 25th harmonic, similar to the ablation of bulk Mo target [Fig. 5(a), the thick curve]. Thus, the electronically driven variations of the delay allowed analyzing the processes attributed to the modification of the ionic transitions of plasma components leading to the enhancement of some harmonics, in contrast to the plateaulike shapes of harmonic distribution commonly observed during plasma HHG studies.

The second example of the application of the developed two-laser HHG scheme is related to the analysis of the suitability of very large aggregates for harmonic generation. Below, we analyze the delay dependence of HHG in the plasmas containing the multicomponent

$CH_3NH_3PbBr_3$ perovskite quantum dots produced on the surface of thin perovskite films by 1064 nm, 5 ns heating pulses and appeared on the path of femtosecond driving pulses at notably longer delays from the beginning of ablation (≥ 5 μs). The 150 nm thick perovskite film was prepared using the two-step method.[35] Figure 6(a) shows spectra of the harmonics generated in the plasma containing $CH_3NH_3PbBr_3$ perovskite species appearing in the area of femtosecond pulse propagation at different delays. The analysis of plasma components appearing during ablation of thin films was reported elsewhere.[36] In the present case, we used the two-laser system for analysis of the contribution of different multiatomic perovskite species to the harmonic yield. The strongest harmonics were observed at a delay of 800 ns (thick blue curve), while a relatively weak yield was obtained at a delay time of 6000 ns (thin red curve). Figure 6(b) shows the variations of the 11th harmonic yield from perovskite LPP at different delays between two
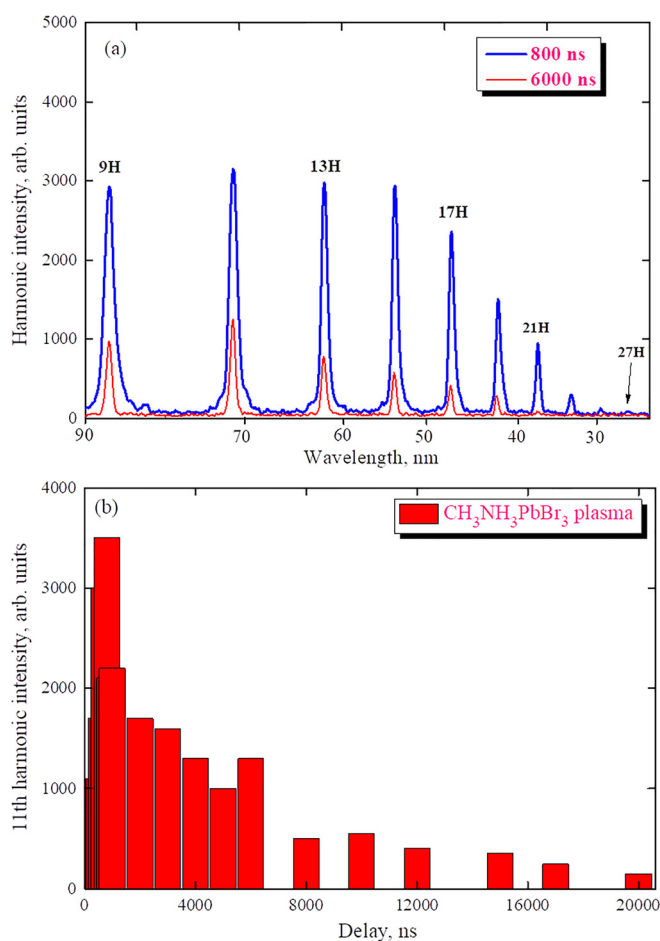

FIG. 6. (a) Harmonic spectra generated during propagation of 40 fs pulses through $CH_3NH_3PbBr_3$ plasma produced on the surface of the thin film. Thick and thin curves correspond to delays of 800 and 6000 ns. (b) Variations of the 11th harmonic intensity at different delays between the heating and driving pulses in the $CH_3NH_3PbBr_3$ LPP. The maximal intensity of the 11th harmonic was obtained at a delay of 800 ns, while the emission of this harmonic was observed along a broad time scale (>20 μs) due to contribution from the large molecular aggregates of perovskites.

laser pulses. The increase in the delay between heating and driving pulses led to a decrease in the harmonic yield, which was observed up to 20 μs. No harmonics were observed at the delays exceeding 25 μs, probably due to the notable decrease in the concentration of LPP.

In previous studies, the restriction of optically modified delays did not allow analyzing the temporally modified contribution of the molecules and their components to the high-order harmonic spectra, particularly, the variations of resonance enhancement for different plasma components. The demonstrated examples of the variable contribution of molecules to high-order harmonic spectra reveal new capabilities of the electronic delay technique, where an optical delay will never be achievable.

In conclusion, the application of the two-laser system approach allows analyzing the slowly spreading plasma, which contains molecular species, on a broad time scale by temporal matching with the propagation of the driving femtosecond pulses through the plasma plume. The advantage of HHG in the plasma created by the nanosecond laser system digitally synchronized with the femtosecond laser system is the delay-dependent analysis of the harmonic yield generated from different components of plasma plumes. Our experiments have demonstrated the dependence of the harmonic yield from different materials on the delay between the heating and driving pulses. The optimal delays for B_4C, ZnO, GaP, GaAs, and Ag_2S plasmas were determined to be approximately 200, 300, 350, 500, and 700 ns, respectively. These variations of delays correspond to the $t \propto (m)^{0.5}$ dependence for both molecular and atomic species. This diagnostic technique can be applied to the analysis of the presence of nanostructures in LPPs through HHG with a high spatiotemporal resolution. We have demonstrated the applicability of the proposed method for analysis of the resonance-enhanced harmonics in atomic and molecular plasmas (Mo and MoS_2) and for studies of the large perovskite aggregates as potential emitters of harmonics. This technique can also be useful for the study of the contribution of different evaporated molecular species for HHG using extremely short pulses. Additionally, the joint application of the harmonic generation and mass-spectroscopy techniques can be considered as a highly versatile tool for *in situ* diagnostics of the laser plasmas containing a large population of the clusters, molecules, and nanoparticles.

REFERENCES

[1] A. L'Huillier and P. Balcou, Phys. Rev. Lett. **70**, 774 (1993).
[2] D. von der Linde and K. Rzàzewski, Appl. Phys. B **63**, 499 (1996).
[3] F. Krausz and M. Ivanov, Rev. Mod. Phys. **81**, 163 (2009).
[4] C. Vozzi, R. Torres, M. Negro, L. Brugnera, T. Siegel, C. Altucci, R. Velotta, F. Frassetto, L. Poletto, P. Villoresi, S. De Silvestri, S. Stagira, and J. P. Marangos, Appl. Phys. Lett. **97**, 241103 (2010).
[5] M. Oujja, R. de Nalda, M. López-Arias, R. Torres, J. P. Marangos, and M. Castillejo, Phys. Rev. A **81**, 043841 (2010).

[6]H. Singhal, V. Arora, B. S. Rao, P. A. Naik, U. Chakravarty, R. A. Khan, and P. D. Gupta, Phys. Rev. A **79**, 023807 (2009).

[7]Y. Pertot, L. B. Elouga Bom, V. R. Bhardwaj, and T. Ozaki, Appl. Phys. Lett. **98**, 101104 (2011).

[8]L. B. Elouga Bom, Y. Pertot, V. R. Bhardwaj, and T. Ozaki, Opt. Express **19**, 3677 (2011).

[9]Y. Pertot, S. Chen, S. D. Khan, L. B. Elouga Bom, T. Ozaki, and Z. Chang, J. Phys. B: At. Mol. Opt. Phys. **45**, 074017 (2012).

[10]S. Haessler, V. Strelkov, L. B. Elouga Bom, M. Khokhlova, O. Gobert, J.-F. Hergott, F. Lepetit, M. Perdrix, T. Ozaki, and P. Salières, New J. Phys. **15**, 013051 (2013).

[11]N. Rosenthal and G. Marcus, Phys. Rev. Lett. **115**, 133901 (2015).

[12]M. A. Fareed, V. V. Strelkov, N. Thiré, S. Mondal, B. E. Schmidt, F. Légaré, and T. Ozaki, Nat. Commun. **8**, 16061 (2017).

[13]M. Wöstmann, L. Splitthoff, and H. Zacharias, Opt. Express **26**, 14524 (2018).

[14]Z. Abdelrahman, M. A. Khohlova, D. J. Walke, T. Witting, A. Zair, V. V. Strelkov, J. P. Marangos, and J. W. G. Tisch, Opt. Express **26**, 15745 (2018).

[15]M. A. Fareed, V. V. Strelkov, M. Singh, N. Thiré, S. Mondal, B. E. Schmidt, F. Légaré, and T. Ozaki, Phys. Rev. Lett. **121**, 023201 (2018).

[16]R. A. Ganeev, *High-Order Harmonic Generation in Laser Plasma Plumes* (Imperial College Press, London, 2012).

[17]R. de Nalda, M. Lopez-Arias, M. Sanz, M. Oujja, and M. Castillejo, Phys. Chem. Chem. Phys. **13**, 10755 (2011).

[18]I. Lopez-Quintas, M. Oujja, M. Sanz, M. Martìn, R. A. Ganeev, and M. Castillejo, Appl. Surf. Sci. **278**, 33 (2013).

[19]J. J. Camacho, M. Oujja, M. Sanz, A. Martìnez-Hernandez, I. Lopez-Quintas, R. de Nalda, and M. Castillejo, J. Anal. At. Spectrom. **34**, 489 (2019).

[20]D. W. Hahn and N. Omenetto, Appl. Spectrosc. **64**, 335A (2010).

[21]M. Oujja, M. Sanz, F. Agua, J. F. Conde, M. García-Heras, A. Dávila, P. Oñate, J. Sanguino, J. R. Vázquez de Aldana, P. Moreno, M. A. Villegas, and M. Castillejo, J. Anal. At. Spectrom. **30**, 1590 (2015).

[22]R. A. Ganeev, G. S. Boltaev, K. Zhang, P. V. Redkin, S. K. Maurya, M. Venkatesh, Z. Yu, V. V. Kim, and C. Guo, OSA Continuum **2**, 1510–1523 (2019).

[23]M. Oujja, I. Lopez-Quintas, A. Benítez-Cañete, R. de Nalda, and M. Castillejo, Appl. Surf. Sci. **392**, 572 (2017).

[24]B. Verhoff, S. S. Harilal, J. R. Freeman, P. K. Diwakar, and A. Hassanein, J. Appl. Phys. **112**, 093303 (2012).

[25]M. Masnavi, M. Nakajima, K. Horioka, H. P. Araghy, and A. Endo, J. Appl. Phys. **109**, 123306 (2011).

[26]W. Marine, J. M. Scotto d'Aniello, and M. Gerri, Mater. Sci. Eng. B **13**, 57 (1992).

[27]J. P. Zheng, Z. Q. Huang, D. T. Shaw, and H. S. Kwok, Appl. Phys. Lett. **54**, 280 (1989).

[28]S. M. Park and J. Y. Moon, J. Appl. Phys. **86**, 7139 (1999).

[29]P. B. Corkum, Phys. Rev. Lett. **71**, 1994–1997 (1993).

[30]M. Lewenstein, P. Balcou, M. Y. Ivanov, A. L'Huillier, and P. Corkum, Phys. Rev. A **49**, 2117–2132 (1994).

[31]D. B. Milošević, J. Phys. B **40**, 3367–3376 (2007).

[32]V. Strelkov, Phys. Rev. Lett. **104**, 123901 (2010).

[33]M. Tudorovskaya and M. Lein, Phys. Rev. A **84**, 013430 (2011).

[34]R. A. Ganeev, H. Singhal, P. A. Naik, V. Arora, U. Chakravarty, J. A. Chakera, R. A. Khan, P. V. Redkin, M. Raghuramaiah, and P. D. Gupta, J. Opt. Soc. Am. B **23**, 2535 (2006).

[35]R. A. Ganeev, K. S. Rao, Z. Yu, W. Yu, C. Yao, Y. Fu, K. Zhang, and C. Guo, Opt. Mater. Express **8**, 1472 (2018).

[36]G. S. Boltaev, R. A. Ganeev, P. S. Krishnendu, K. Zhang, and C. Guo, Sci. Rep. **9**, 11414 (2019).